

The key role played by mesoporous alumina as binder for obtaining ultra-hard CaO based pellets for thermochemical heat storage leveraging the CaO/CaCO₃ cycle

D. Castro-Yáñez^a, M. Erans^{a,b}, A. Peral^a, R. Sanz^a, J. González-Aguilar^c, M. Romero^c, L. Briones^{a,**}, E.S. Sanz-Pérez^{a,***}, J.M. Escola^{a,*}

^a Group of Chemical and Environmental Engineering, Rey Juan Carlos University, C/ Tulipán s/n, 28933, Móstoles, Spain

^b Department of Chemical Engineering, Universitat de València, Avinguda de l'Universitat, 46100, Burjassot, Valencia, Spain

^c Unit of High Temperature Processes, IMDEA Energy Institute, Avda. Ramón de la Sagra 3, 28935, Móstoles, Spain

ARTICLE INFO

Handling Editor: Panos Seferlis

Keywords:

Thermochemical heat storage

CaO/CaCO₃ cycle

Calcium looping

Mesoporous alumina

CST

ABSTRACT

The synthesis of CaO-based pellets with high energy storage and suitable mechanical resistance after prolonged cycling is pivotal for the successful implementation of the Calcium looping (CaL) technology for energy storage in CSP plants. In this work, CaO-based spherical pellets (CAA) were prepared made up of 60 wt % Ca(OH)₂ and varying ratios (0–40 wt %) of commercial γ -Al₂O₃ and mesoporous γ -Al₂O₃ (m-Al₂O₃). They were tested in TG in several CO₂ carbonation/decarbonation cycles (15 and 50 for selected pellets) and their respective average crushing strengths measured. After 15 cycles, the optimum pellet CAA 20-20 (60 wt % Ca(OH)₂/20 wt % γ -Al₂O₃/20 wt % m-Al₂O₃) exhibits a remarkable energy storage density of 1030 kJ/kg with a superb crushing strength of ~29 N. This was ascribed to the enhanced formation of the calcium aluminate mayenite (Ca₁₂Al₁₄O₃₃), since the high BET surface area (384 m² g⁻¹) of mesoporous γ -Al₂O₃ promotes the interaction with calcium oxide. Additionally, CAA 20-20 showed meaningful porosity that favored CO₂ mass transport. Interestingly, after 50 cycles, the optimum CAA 20-20 pellet maintained a high carbonation yield (0.46), representing an 84 % of the initial value and corresponding to an energy storage density of ~873 kJ/kg. Additionally, the optimum CAA 20-20 pellet was coated with an external layer of Al-MCM-41 silica that augmented its crushing strength up to 37 N, with a concurrent slight abatement in the carbonation yield and energy storage density after 50 cycles (0.43 and ~824 kJ/kg). Consequently, both uncoated and coated CAA 20-20 pellet are promising for the successful implementation of CaL in CSP plants.

1. Introduction

The large-scale deployment of concentrated solar power (CSP) for electricity generation relies heavily on the development of suitable storage systems that can effectively overcome the intermittency of solar power, which distinctly hinders the adaption of solar power supply to demand (Liu et al., 2018). In this respect, thermal energy storage (TES) technology has emerged as a promising means to solve this shortcoming for CSP plants with the added advantage of reducing CO₂ emissions as well as by replacing electricity generated by fossil fuels (Xu et al., 2014). There are three different technologies for thermal energy storage:

sensible heat storage (Hasnain, 1998), latent heat storage (Opolot et al., 2022), and thermochemical heat storage (Islam et al., 2018) with a large number of candidate reactions (Yan et al., 2015), the latter being particularly advantageous due to its superior energy density (five to ten-fold) (Pardo et al., 2014). Currently, the existing second-generation tower CSP plants harness both sensible and latent heat storage by means of molten salts which are subsequently used to generate steam to be fed to a thermal plant operating through a Rankine cycle (Rea et al., 2018). However, this design usually faces corrosion problems that undermine their performance due to phase change materials (Vasu et al., 2017), molten salt (Bell et al., 2019) or molten chlorides (Lambrecht et al.,

* Corresponding author.

** Corresponding author.

*** Corresponding author.

E-mail addresses: laura.briones.gil@urjc.es (L. Briones), eloy.sanz@urjc.es (E.S. Sanz-Pérez), josemaria.escola.saez@urjc.es (J.M. Escola).

<https://doi.org/10.1016/j.jclepro.2024.141702>

Received 3 January 2024; Received in revised form 15 February 2024; Accepted 6 March 2024

Available online 7 March 2024

0959-6526/© 2024 The Authors. Published by Elsevier Ltd. This is an open access article under the CC BY-NC-ND license (<http://creativecommons.org/licenses/by-nc-nd/4.0/>).

2022). In this regard, the forthcoming third generation CSP plants are envisaged to be based on supercritical (sCO₂) Brayton cycles (Chen et al., 2022) which take advantage of their higher efficiency in electricity conversion although at the expense of higher working temperatures (around 700 °C) (García-Ferrero et al., 2022). Therefore, the success of these third generation CSP plants requires the implementation of higher energy density materials based on thermochemical heat storage, capable of operating at temperatures above 700 °C.

Thermochemical heat storage (TCHS) is based on a reversible reaction that soaks up solar energy in the endothermic step and releases heat in the exothermic step with a high reaction enthalpy and no side reactions (Prieto et al., 2016). This yields high energy storage (0.5–3 GJ m⁻³) with low heat losses, enabling long storage periods (Carrillo et al., 2019) working with non-toxic gases (Gollsch and Linder, 2023). For a suitable storage operation, the kinetics of both transformations are meant to occur fast, and the reaction products must be stable, non-toxic, abundant, and with low cost (Gil et al., 2010). Additionally, to generate electricity with high efficiency in CSP plants, the chosen reversible reaction for TCHS should take place at high temperatures (Ervin, 1977). One of the most promising candidates is the cycle CaCO₃/CaO (Müller et al., 2011) due to its remarkably high reaction enthalpy with little dependency on reaction temperature. This fact renders it as one of the largest theoretical energy storage systems reported (3.2 GJ m⁻³) (Abedin, 2011), with the advantage of the abundance of potential cheap sources such as limestone (Abanades et al., 2005). The associated reversible reaction is shown as follows:



The CaCO₃/CaO cycle has been put forward to work through a Calcium Looping process (CaL) (Perejón et al., 2016) for a large-scale CO₂ capture (Blamey et al., 2010) with a fluid-bed reactor (Shimizu et al., 1999) and several sorbents (Erans et al., 2016) integrated within CSP plants. Thus, concentrated solar power facilitates the endothermic reaction in a solar calciner releasing CO₂ and CaO, which are stored separately (Ortiz et al., 2019). Subsequently, both reagents are combined in a carbonator, releasing the heat of the reverse carbonation reaction, which is used in a power cycle. In this regard, CSP-CaL systems have been fully integrated by coupling the CaL process to a closed loop CO₂ Brayton cycle, achieving an overall thermal efficiency around 46% (Chacartegui et al., 2016) that was further optimized by an additional 5% (Alovisio et al., 2017). It is noteworthy that these efficiency values slightly exceed those reported for open CO₂/air Brayton cycles (Edwards and Materić, 2012).

However, the main drawback of the CSP-CaL process is the decay in heat storage performance of the limestone-derived CaO over repeated cycles, which is mostly due to the sintering of the CaCO₃ particles at the high decarbonation temperatures (700–900 °C) (Grasa and Abanades, 2006). This is accompanied by a distinct volume change (16.7 and 36.9 cm³ g⁻¹ for CaO and CaCO₃, respectively) and by pore plugging during carbonation as well (Salvador et al., 2003) in several sorbents (Kierzkowska et al., 2013). Thus, during CaO carbonation, initially a fast stage (controlled by chemical kinetics) takes place, followed by a slower stage (controlled by diffusion), which is ascribed to the formation of an outer CaCO₃ surface layer over the CaO grains, resulting in significantly slower diffusion rates (0.003 cm² s⁻¹ for CaCO₃ and 0.3 cm² s⁻¹ for CaO, respectively) (Choi et al., 2009). Hence, the carbonation process at 600 °C stalled over commercial CaO wherein the formation of an outer CaCO₃ layer with a thickness of 90 nm was observed. Strikingly, this phenomenon was absent in sol-gel CaO because of the presence of abundant mesopores (Sun et al., 2019).

Several strategies have been devised to improve the cycling stability of the CaL process, such as doping with diverse additives, steam treatment, and modification of the porosity. They are mostly focused on enhancing the sintering resistance of the solids and averting their agglomeration as well, being successful in different ways. Thus, the doping

with diverse additives with high Tamman temperatures, such as Al₂O₃ and different calcium aluminates (Ca₉Al₆O₁₈, Ca₁₂Al₁₄O₃₃) (Zhou et al., 2012), alumina cement (Morona et al., 2019), SiO₂ (Chen et al., 2018), MnO₂ (Sun et al., 2012), TiO₂ (Chen et al., 2016a), ZrO₂ (Broda and Müller, 2014) and CeO₂ (Wang et al., 2015) has been reported. In addition, binary doping with Fe/Mn and the incorporation of Zr as stabilizer improved not only the cycling stability of the CaO/CaCO₃ couple but also increased their spectral absorption performance through the formation of dark spots composed of Ca₂Fe₂O₅ and Ca₄Mn₃O₁₀. This development is highly promising for further application in CSP plants (Sun et al., 2022). Likewise, a multi-doping strategy was applied for the sol-gel synthesis of CaO-based composites. The addition of Ce, Co, and Mn improved both optical absorption and cycling stability (Da and Zhou, 2022). On the other hand, steam treatment has also proven effective in retrieving and even restoring the carbonation performance of the CaL process by increasing the porosity of the solids crafted, for example, by sol-gel technique (Chen et al., 2016b) or with another reactions (Bian et al., 2022) through the formation of more cracks and channels (Sun et al., 2020). Similarly, MgO-stabilized nano CaO was prepared using a citric acid-based carbon template that, after removal by pyrolysis, enhances porosity, leading towards a remarkable long-term performance during the cycling (Wang et al., 2020).

In previous works, Ca(OH)₂/γ-Al₂O₃ (60/40 w/w) pellets were prepared and covered with mesoporous alumina and silica coatings in order to enhance their mechanical resistance in CaO/Ca(OH)₂ dehydration/hydration cycles. This research was aimed at harnessing the exothermic hydration reaction for energy storage in CSP plants implementing either fixed (Valverde-Pizarro et al., 2020) or moving beds technology (Briones et al., 2022). Hence, the coating enabled both the maintenance of pellet integrity along the successive cycles and the preservation of high hydration capacity by preserving the porosity of the pellets. However, the lower energy storage of the hydration reaction of CaO (104 kJ mol⁻¹) makes more promising explore the carbonation reaction instead. In this work, Ca(OH)₂ based pellets have been prepared by substituting either partially or totally the γ-Al₂O₃ binder with mesoporous γ-Al₂O₃ and their performance has been tested in successive CaO/CaCO₃ cycles, determining the carbonation yields and the related energy storage density. This substitution is aimed at exploring the energy storage performance of the pellets along cycling as well as its mechanical integrity ascertaining the role played by the remarkable textural properties of mesoporous γ-Al₂O₃. In this respect, the high BET surface area and mesoporosity of mesoporous γ-Al₂O₃ is expected to have several positive effects upon the CaO-based pellets. Firstly, the enhanced porosity will allow faster CO₂ mass transport inside and outside the pellets, leading towards higher carbonation yields. Secondly, the high BET surface area of the CaO-based pellets will facilitate the interaction of mesoporous γ-Al₂O₃ with calcium oxide, which will favor the formation of different calcium aluminates. These compounds will increase the mechanical resistance of the CaO-based pellets, slowing down as well the sintering of the calcium oxide/calcium carbonate particles. This is particularly important since it will enable to hold high carbonation yields after prolonged cycling. On the other hand, this is the first time mesoporous γ-Al₂O₃ has been investigated as binder of the CaO-based pellets since previously it has been only harnessed as coating of the pellets (Valverde-Pizarro et al., 2020). Additionally, the usage of mesoporous γ-Al₂O₃ as binder will certainly enable to make strides to improve the trade-off between the increasing hardness and a sizeable energy storage density of the CaO-based pellets. Furthermore, a mesoporous silica-alumina coating was deposited over an optimal pellet composition (60 Ca(OH)₂/20 γ-Al₂O₃/20 mesoporous γ-Al₂O₃, w/w/w) to assess its influence on mechanical integrity and cycling performance.

2. Materials and methods

2.1. Chemicals

Commercial calcium hydroxide ($\text{Ca}(\text{OH})_2$, 98 wt %, Acros Organics) and commercial alumina ($\gamma\text{-Al}_2\text{O}_3$, 90 wt %, Merck) were chosen to manufacture the pellets. For the synthesis of mesoporous $\gamma\text{-Al}_2\text{O}_3$, the following chemicals were used: aluminium isopropoxide (99 wt %, Aldrich), hexadecyltrimethylammonium bromide (99 wt %, Aldrich), isopropanol (99.8 wt %, Scharlau), and hydrochloric acid (37 wt % aqueous solution, Honeywell). The chemicals used to synthesize the mesostructured silica-alumina gel (Al-MCM-41) for coating were hexadecyltrimethylammonium bromide (99 wt %, Aldrich), aluminium chloride hexahydrate (99 wt %, Aldrich), tetraethyl orthosilicate (98 wt %, Aldrich), and dimethylamine (40 wt % in H_2O , Aldrich).

Mesoporous alumina ($\text{m-Al}_2\text{O}_3$) was synthesized by a sol-gel synthesis procedure with cationic surfactants published elsewhere (Aguado et al., 2005, 2010) and outlined in the Supporting information (SI, cf. Fig. S2). Additionally, the coating of some chosen pellets was performed using a mesostructured silica-alumina gel, prepared following a procedure published in the literature for the synthesis of Al-MCM-41 (Lin et al., 1999), also detailed in the SI.

2.2. Pellets manufacturing

Mesoporous $\gamma\text{-Al}_2\text{O}_3$, commercial $\gamma\text{-Al}_2\text{O}_3$, and $\text{Ca}(\text{OH})_2$ powders were used to prepare the core of spherical pellets (Briones et al., 2022). $\text{Ca}(\text{OH})_2$ was harnessed as the pellet base, and the different aluminas were used as binders to provide porosity and mechanical strength (Valverde-Pizarro et al., 2020). The same proportion of $\text{Ca}(\text{OH})_2$ was always loaded in all cases for pellet manufacturing (60 wt %), with the remaining 40 wt % corresponding to the aluminas. The share of $\text{m-Al}_2\text{O}_3$ was varied within 0–40 wt %, with the remainder amount up to 40 wt % corresponding to the commercial $\gamma\text{-Al}_2\text{O}_3$. These materials were mixed and crushed in a mortar to obtain a homogeneous mixture, and the final powder was put into contact with miliQ water to form a malleable paste. Spherical pellets (around 40) were hand-shaped to achieve diameters between 2.5 mm and 3 mm. In previous experiments it was determined that, for spherical pieces, the dip-coating procedure was more effective for this size interval, since the thickness of the gel layer deposited on the pellet surface is highly influenced by the diameter of the pellet. For an actual application, however, the shape and size of the pieces should be adjusted to ensure that the reactor bed can be fluidized without an excessive pressure drop.

The obtained pellets were denoted as CAA x-y where x stands for the weight share of commercial $\gamma\text{-Al}_2\text{O}_3$ and y represents the percentage of $\text{m-Al}_2\text{O}_3$, respectively. Accordingly, the following pellet samples were prepared: CAA 40-0, CAA 30-10, CAA 20-20, CAA 10-30, and CAA 0-40.

2.3. Pellets coating

Once the mesostructured silica-alumina gel was prepared, uncalcined pellets were individually immersed in it for a few seconds to apply the coating. The pellets were placed in a steel grid with a handle prior to immersion, so most of the surface could be in contact with the gel. After about 2 s, the grid was extracted from the gel very slowly to allow extra gel to drip off. This ensures a more uniform coating and prevents the formation of thick coating patches that would easily detach from the cores. There are several industrial dip-coating processes that could likely mimic our results, so this procedure could actually be applied on a larger scale.

Subsequently, both uncoated and coated pellets were dried in an oven at 110 °C for 1 h for a controlled removal of the solvent. Finally, they were calcined under static air in a furnace firstly at 80 °C for 2 h and then at 600 °C for 3 h. CAA 20-20 pellets were coated with porous silica-alumina and the formed material was denoted as CAA 20-20 M.

Fig. 10 illustrates the whole process of preparation of both uncoated and coated pellets:

2.4. Sample characterization

The different crystalline phases present in the pellets were determined by powder XRD technique on a Phillips X'Pert MPD diffractometer. Prior to XRD analyses, the pellets were crushed in a mortar to obtain a fine powder. The measurements were performed using $\text{Cu-K}\alpha$ radiation with a counting time of 1 s and a step size of 0.1°. Crystalline structures were identified by means of the X'Pert High Score Plus software.

The textural properties of the pellets were calculated from their N_2 adsorption/desorption isotherms at -196.15 °C carried out on a Micromeritics TRISTAR 3000 device, using between 5 and 8 pellets of every type. Pellets were outgassed before each analysis, initially at 90 °C for 30 min and then at 200 °C for 480 min. The analyses were always carefully performed to prevent pellet cracking. The Brunauer-Emmett-Teller method (BET) (Brunauer et al., 1938) was applied to the adsorption branch of the isotherms to calculate the specific surface area of samples, while their pore volume was obtained by measuring at $p/p_0 = 0.98$. In addition, the pore size distribution was determined by means of the Barrett-Joyner-Halenda method (BJH) (Barrett et al., 1951) applied to the adsorption branch of the isotherm.

The composition and morphology of the pellets were determined using Scanning Electron Microscopy (SEM) on a Hitachi TM-100 equipment, equipped with an energy-dispersive X-ray spectroscopy (EDX) detector. The pellets were placed on the sample holder using a carbon adhesive disc to avoid any rolling and to prevent any powder particles being dragged by the high vacuum. The samples were observed without applying any conductive coating. The images were collected of the initial pellets (after calcination) and at the ending of the carbonation cycles. Likewise, micrographs were collected outside and inside the pellets to check both the coating and the inner porous structure, respectively. To expose the inner part, the pieces were carefully broken into halves applying pressure. EDX analyses were performed to check the particular composition at some specific points.

The average mechanical crushing strength of the pellets was measured on a Chatillon MT Ametek dynamometer equipment, using 15 pellets of every sample and obtaining the standard deviation. The analyses were carried out both before and after the decarbonation/carbonation cycles. This particular reaction system was chosen because of its high versatility, since the thermobalance allows performing a large number of cycles, easily changing the temperature and gas inlet. Besides, the precision of the mass measurement is on the microgram level. From an actual operational approach, this versatility is also needed. Since the intended application of this investigation is to provide energy storage materials for third generation open-cycle CSP plants, high decarbonation (>700 °C) and carbonation temperatures (>600 °C) are required. Reaching such high temperatures combined with a continuous gas flow would need a robust tubular furnace with separate gas inlets for CO_2 and N_2 . Besides, the mass measurements of the TG can easily be converted into carbonation yields. Otherwise, a continuous analysis system for the outlet gases would be required. Any alternative reaction setup would be much more complicated to operate and would probably require the cooling down of the sample to change from carbonation to decarbonation, limiting the number of cycles that could be carried out. Thus, for the screening of a variety of materials, a TG setup seems to be reasonable reaction system, although any future insight on an actual TES system should be performed in a more realistic one.

In this regard, the number of carbonation/decarbonation cycles initially performed for every sample was 15, while a higher number of cycles (50) was conducted over some chosen pellets to provide a longer-term assessment. The yield (X_c) of the carbonation stages in each cycle was calculated following Equation (1):

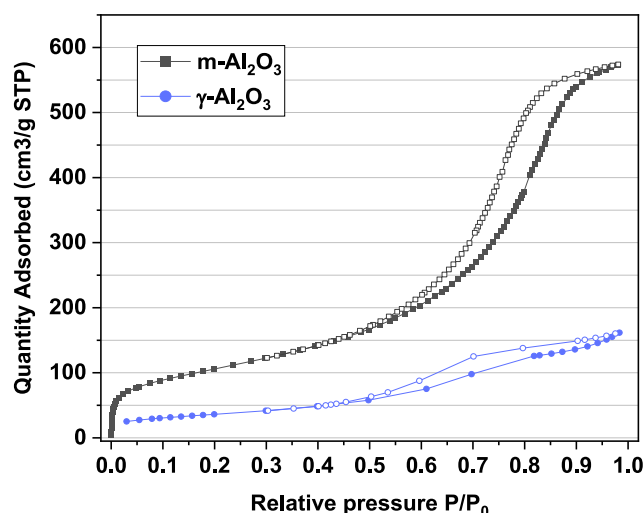


Fig. 1. N₂ adsorption-desorption isotherms at -196.15 °C of the mesoporous and commercial alumina binders.

Table 1

Textural properties of the calcined CAA pellets ($\text{Ca}(\text{OH})_2/\gamma\text{-Al}_2\text{O}_3/\text{m-Al}_2\text{O}_3$) and alumina binders obtained from nitrogen physisorption analyses at -196.15 °C. Alumina samples analysed in powder form. CAA samples analysed in pellet form.

Sample	BET surface area (m^2/g)	Total volume of pores (cm^3/g)
$\gamma\text{-Al}_2\text{O}_3$	130	0.25
m- Al_2O_3	384	0.89
CAA 40-0	52	0.12
CAA 30-10	47	0.11
CAA 20-20	40	0.09
CAA 10-30	17	0.03
CAA 0-40	1	0.00
CAA 20-20 M	50	0.09

$$X_e = \frac{TG \text{ maximum} - TG \text{ minimum mass}}{\text{maximum } CO_2 \text{ mass}} \quad 1$$

Where TG maximum mass is the highest mass value detected for any given cycle at the end of the carbonation stage at 600 °C and TG minimum mass is the lowest mass value at the end of the of the previous decarbonation stage at 850 °C, for a cycle is considered to start with decarbonation and end with carbonation. These points were devised after plotting the raw data. Thus, the subtraction accounts for the actual CO_2 uptake for that particular sample and cycle. The maximum CO_2 mass uptake was calculated considering the complete stoichiometric carbonation of the theoretical CaO amount in one pellet – the actual mass of the analysed pellet is known –, taking into consideration the theoretical initial 60 % load of $\text{Ca}(\text{OH})_2$ as well as a purity of 92 %, which was deduced from previous analyses performed for the pure commercial $\text{Ca}(\text{OH})_2$ powder. The mass of the coating, which was previously determined to be $<3\%$ of the total mass of the pellet by gravimetric measurements, was disregarded. Thus, the yield of the carbonation stage may vary within the 0 – 1 range.

On the other hand, the energy storage densities (TESD) per kilogram of sample were calculated using the obtained conversions and the enthalpy of the carbonation reaction ($178.29 \text{ kJ mol}^{-1}$), according to Equation (2):

$$TESD \left(\frac{\text{kJ}}{\text{kg sample}} \right) = \left(178.29 \frac{\text{kJ}}{\text{mol}} \right) * X_e * \frac{\text{Maximum } CO_2 \text{ mass (kg } CO_2)}{\text{Pellet mass (kg sample)}} * \frac{1 \text{ mol } CO_2}{0.04401 \text{ kg } CO_2} \quad 2$$

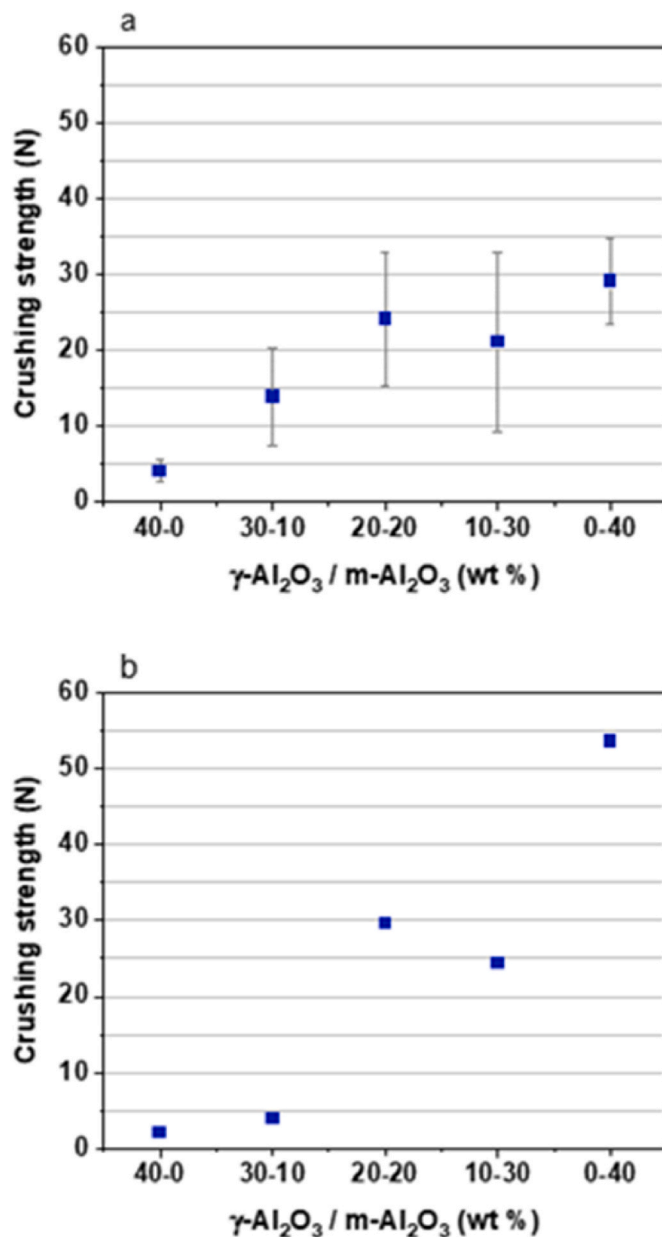


Fig. 2. Crushing strength of the calcined CAA ($\text{Ca}(\text{OH})_2/\gamma\text{-Al}_2\text{O}_3/\text{m-Al}_2\text{O}_3$) pellets. Average values and standard deviations for pellets before (a) and after (b) 15 carbonation/decarbonation cycles.

3. Results and discussion

3.1. Effect of the amount of mesoporous alumina

As stated before, the main goal in adding mesoporous alumina to the composition of the $\text{Ca}(\text{OH})_2/\gamma\text{-Al}_2\text{O}_3$ cores was to increase the mechanical resistance of the pellets and their longevity under realistic operation conditions for CaL applications in CSP plants (decarbonation at 800 – 900 °C and carbonation at 500 – 650 °C). The commercial acid $\gamma\text{-Al}_2\text{O}_3$ used in previous works for dehydration/hydration cycles provided a noticeable increase in the crushing strength of the pellets, up to 10 N compared to <2 N for the pure $\text{Ca}(\text{OH})_2$ (Valverde-Pizarro et al., 2020). However, there was little evidence of an actual interaction between the alumina and the calcium oxide since XRD analyses did not show any Ca–Al mixed phases, likely because of the lower reaction temperatures compared to decarbonation/carbonation, but also because of a low reactivity of the commercial alumina as well. Moreover, in order

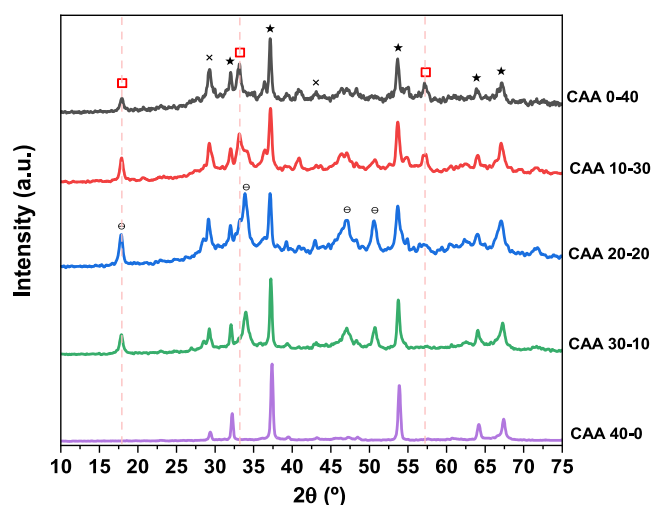


Fig. 3. XRD patterns of the calcined CAA ($\text{Ca}(\text{OH})_2/\gamma\text{-Al}_2\text{O}_3/\text{m-Al}_2\text{O}_3$) pellets showing the main reflections of lime (★), portlandite (⊖), calcite (x), and mayenite (□ and dashed line).

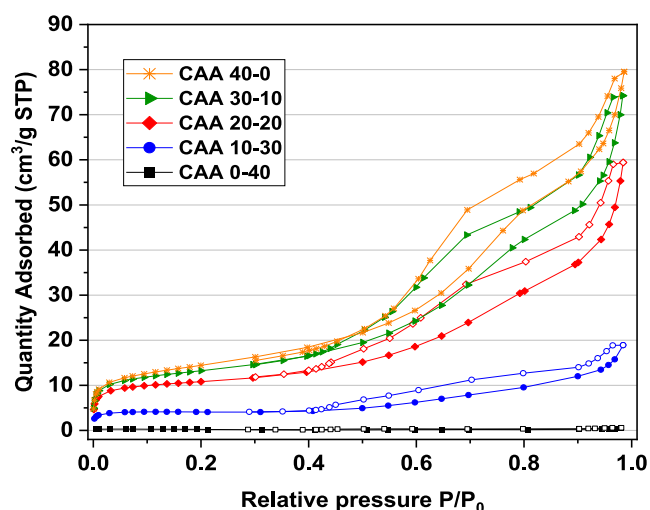


Fig. 4. N_2 adsorption-desorption isotherms at -196.15°C of the calcined CAA ($\text{Ca}(\text{OH})_2/\gamma\text{-Al}_2\text{O}_3/\text{m-Al}_2\text{O}_3$) pellets.

to prepare the pellets for the carbonation/decarbonation cycle, a higher calcination temperature had to be applied. For the dehydration/hydration cycle pellets were calcined at 500°C , while calcium looping is performed at higher temperatures, so calcination at 600°C was required to stabilize the samples before cycling. However, the reactions occurring at this higher temperature provided more fragile pellets compared to the previous ones – as it will be shown later – and made the original 60 wt% $\text{Ca}(\text{OH})_2$ -40 wt% $\gamma\text{-Al}_2\text{O}_3$ inadequate for the intended application.

N_2 adsorption-desorption isotherms at -196.15°C for the alumina binders are depicted in Fig. 1, whereas the specific surface areas and total porosities are shown in Table 1. It can be inferred that the commercial alumina is rather porous, displaying a specific surface area of $130\text{ m}^2/\text{g}$ and a total porosity of $0.25\text{ cm}^3/\text{g}$, with pores of various sizes centered at around 8 nm. Mesoporous alumina reached a BET surface area of $384\text{ m}^2/\text{g}$ and a total volume of pores of $0.89\text{ cm}^3/\text{g}$, with a narrower distribution of pores centered at 12 nm. These textural properties widely exceed those of the commercial alumina due to the presence of a surfactant in the synthesis gel of the mesostructured sample.

Thus, mesoporous alumina ($\text{m-Al}_2\text{O}_3$), provides a higher surface area (Aguado et al., 2005), so an enhanced contact between the two

components (calcium oxide/carbonate and mesoporous alumina) takes place and, therefore, a more intense chemical reaction was expected at the high temperatures of decarbonation/carbonation cycles. These features of mesoporous alumina would ease the formation of some hard-crystalline calcium aluminates in a larger extent than the commercial alumina which is meant to provide mechanical resistance to the pellet although at the expense of a certain abatement of carbonation yield and thereby, energy storage density. On the other hand, these alumina binders also provide a certain macro/mesoporosity to the pellets, so they facilitate the CO_2 mass transport to and from the core. This porosity is to be maintained or the pellets would crack during the CO_2 release. Hence, a trade-off between crushing strength and porosity must be reached avoiding an excessive calcium aluminates formation as well.

In order to determine the most adequate composition of the cores, a fixed amount of $\text{Ca}(\text{OH})_2$ (60 wt %) was mixed with different $\gamma\text{-Al}_2\text{O}_3/\text{m-Al}_2\text{O}_3$ combinations. 40 wt % $\gamma\text{-Al}_2\text{O}_3/0$ wt % $\text{m-Al}_2\text{O}_3$ was named as CAA 40-0 and 0 wt % $\gamma\text{-Al}_2\text{O}_3/40$ wt % $\text{m-Al}_2\text{O}_3$ was named as CAA 0-40. The other samples were CAA 30-10, CAA 20-20 and CAA 10-30. These mixtures were conformed into spherical pieces around 3 mm in diameter, dried and calcined.

The mechanical resistance of the pellets was checked by crushing at least 15 pieces of each sample in a dynamometer. The average crushing strength values and their corresponding standard deviations are shown in Fig. 2 a. The reference sample, CAA 40-0 (40% commercial $\gamma\text{-Al}_2\text{O}_3$ and no $\text{m-Al}_2\text{O}_3$), exhibited a very low value, below 5 N. Crushing strength was dramatically increased by substituting 10 % of the commercial alumina for $\text{m-Al}_2\text{O}_3$, achieving up to 14 N, and reaching values over 20 N with the other mixtures. The hardest sample, CAA 0-40, reached almost 30 N, which is an outstanding value regarding those of comparable materials. Although several authors have prepared CaO or $\text{Ca}(\text{OH})_2$ -based pellets for Calcium Looping or dehydration/hydration cycles with different binders (Chen et al., 2012), doping agents or core-shell strategies (Sedghkerdar et al., 2016) aiming to increase mechanical strength, an effective measurement of the resistance of the pieces has not always been given. Even when the resistance to crushing was measured, an equivalent pellet size is needed to compare absolute hardness values. In this regard, most of the reported pellets are much smaller (0.6–1.5 mm) than the pieces described here (2.5–3 mm), and the corresponding crushing strength values are in consequence much lower (ranging from 0.6 to 9 N) (Boyu et al., 2021). F. J. Liu et al. (2006) used clay as a binder to prepare CaO pellets with sizes ranging from 1.4 mm to 4 mm and crushing loads from 15 N to 27 N, increasing with pellet size. Criado et al. (Álvarez Criado et al., 2015) prepared 2 mm $\text{CaCO}_3\text{-Na}_2\text{Si}_3\text{O}_7$ pellets, with resistance to crushing values of 16 N after calcination. Therefore, obtaining 3 mm pieces with a 30 N resistance to crushing is a very promising starting point for practical applications, as long as the mechanical properties can endure throughout the cycles.

The measured crushing strength after cycles is, consequently, a key parameter. To check the evolution of this property, the samples were subjected to 15 consecutive carbonation/decarbonation cycles in a thermo-microbalance at $600^\circ\text{C}/850^\circ\text{C}$, respectively. The recovered pieces were then tested again, and the crushing strength values are presented in Fig. 2 b. After 15 cycles CAA 40-0 and CAA 30-10 were very soft (<5 N) due to the continuous volume changes caused by CO_2 adsorption/release during cycling at high temperatures, which led towards their fragilization. The calcium aluminate that could have been formed during calcination and cycles is not enough to provide any stabilizing effect on the structure because of the low amount of reactive alumina and the relatively mild temperatures applied (Benitez-Guerrero et al., 2018b). In contrast, CAA 20-20 and CAA 10-30 hold their initial mechanical strength, while when the percentage of mesoporous alumina is too high, as in CAA 0-40, the crushing strength rises up to a remarkable 54 N. This result suggests that, in the chosen operation conditions, calcium oxide/carbonate and mesoporous alumina react until the limiting reactant is extensively consumed, which could lead to a continuous deterioration in performance. However, when the amount

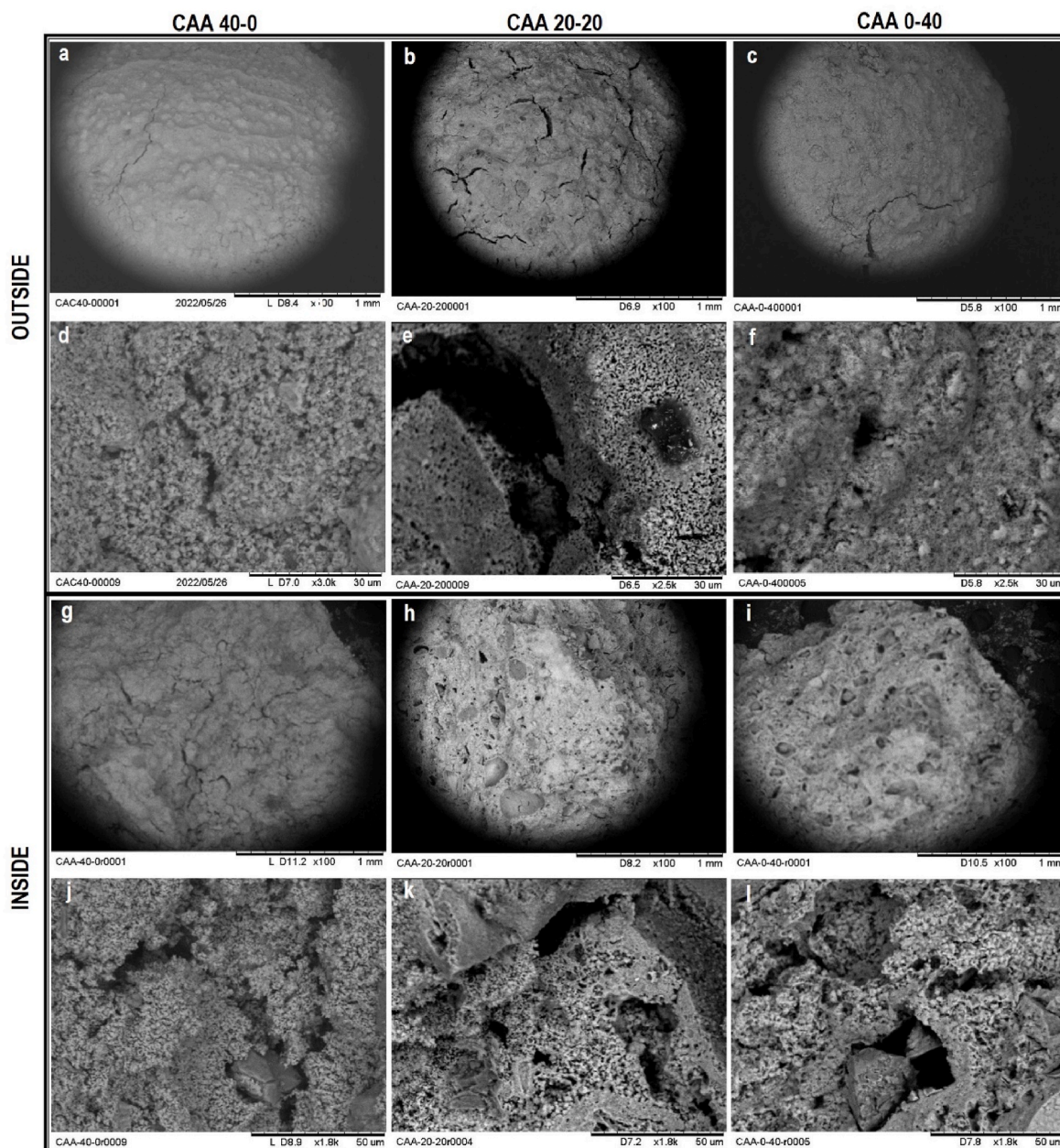


Fig. 5. SEM images of calcined CAA ($\text{Ca}(\text{OH})_2/\gamma\text{-Al}_2\text{O}_3/\text{m-Al}_2\text{O}_3$) pellets: CAA 40-0 (a, d, g, j), CAA 20-20 (b, e, h, k) and CAA 0-40 (c, f, i, l).

of $\text{m-Al}_2\text{O}_3$ is strictly controlled in the 20–30 % range, the initial mechanical properties are not affected by the cycles, so the amount of energy stored is expected to be stable within a narrow interval. This is, of course, a desired behavior, as it not only spans the longevity of the materials, but also allows a more precise design of the energy storage system.

The formation of Ca–Al mixed phases, such as calcium aluminates, by calcination of calcium oxide and aluminium compounds at high temperature has been reported elsewhere (Benitez-Guerrero et al., 2018b). The presence of Ca–Al mixed phases and their specific structures in the calcined CAA pellets was checked by XRD, with the obtained patterns being shown in Fig. 3. The main calcium compound in calcined pellets is CaO (lime structure), as expected after the thermal treatment. $\text{Ca}(\text{OH})_2$ (portlandite) and CaCO_3 (calcium carbonate, calcite) are also observed, with their presence being ascribed to the reaction of calcium oxide with atmospheric water and CO_2 . Additionally, the patterns of all $\text{m-Al}_2\text{O}_3$ containing samples clearly show the main reflections of

mayenite ($\text{Ca}_{12}\text{Al}_{14}\text{O}_{33}$) at $2\theta \approx 18^\circ$, 33° and 57° . Interestingly, the share of mayenite tends to increase with the loaded amount of $\text{m-Al}_2\text{O}_3$. Mayenite is a naturally occurring mesoporous calcium aluminate with the chemical composition $\text{Ca}_{12}\text{Al}_{14}\text{O}_{33}$ and a distinct hardness. It is widely used in the cement industry, as a dental ceramic, and as a component of optical and electronical devices. Hence, it seems that the formation of mayenite is the responsible for the enhanced crushing strength values observed with the increasing share of $\text{m-Al}_2\text{O}_3$ in the pellets (Manovic and Anthony, 2011). Then, both the high BET surface area and low grain size of mesoporous alumina would explain the favored formation of mayenite in these pellets.

In previous work using commercial $\gamma\text{-Al}_2\text{O}_3$ as a binder, the CaO pellets presented specific surface areas of around $60 \text{ m}^2/\text{g}$ and pore volumes between $0.13 \text{ cm}^3/\text{g}$ and $0.16 \text{ cm}^3/\text{g}$, with both mesopores and macropores. The aim of using mesoporous alumina is to enhance resistance to crushing while maintaining the porosity needed for mass transfer during cycles. The porosity of the CAA mixed cores offered

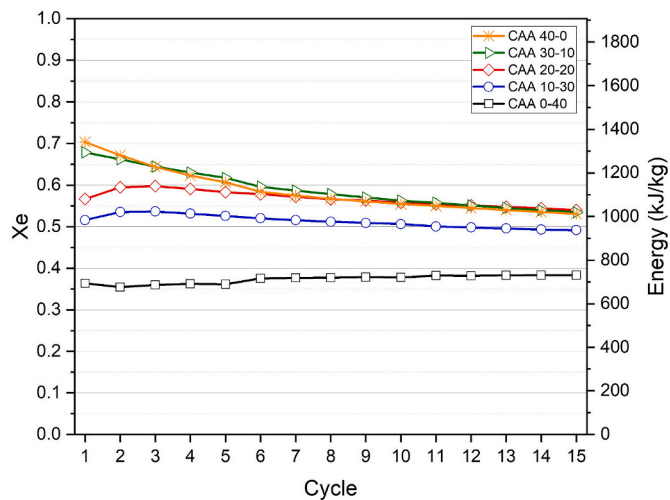


Fig. 6. Carbonation yield (X_e) (left) and energy storage density (kJ/kg) (right) of the different calcined CAA ($\text{Ca}(\text{OH})_2/\gamma\text{-Al}_2\text{O}_3/\text{m-Al}_2\text{O}_3$) pellets along 15 carbonation/decarbonation cycles.

different results, as depicted in Fig. 4 and Table 1. The pellets containing only $\gamma\text{-Al}_2\text{O}_3$ (CAA 40-0), present a surface area of just $52 \text{ m}^2/\text{g}$ and a total pore volume of $0.12 \text{ cm}^3/\text{g}$, which are in agreement with the previously reported results. Substituting up to 20 % of the commercial alumina with the mesoporous ones causes a moderate reduction of the surface area and pores volume to $40 \text{ m}^2/\text{g}$ and $0.09 \text{ cm}^3/\text{g}$, but higher m- Al_2O_3 contents collapse the porous structure and CAA 0-40 is virtually a completely dense sample. These results agree with the increasing formation of mayenite within samples with higher shares of m- Al_2O_3 .

The general aspect (granulometry, presence of large voids or cracks, etc.) of the CAA samples was determined by scanning electron microscopy. The samples were analysed from the outside and then broken in halves to photograph the inner structure. A collection of images corresponding to CAA 40-0, CAA 20-20, and CAA 0-40 is shown in Fig. 5. From the outside (images a, b, and c) the three samples look similar; the appearance is homogeneous, and the pieces appear cohesive, showing only small and superficial cracks formed during calcination. A higher magnification (images d, e, and f) allows observing the texture created by the granulometry of CaO. On the other hand, the inside images (g, h, and i) show evidence of the formation of CO_2 and steam bubbles during calcination in CAA 20-20 and CAA 0-40. The harder structure derived from the formation of mayenite hinders the fast release of gases, hence being accumulated and forming large cavities. This effect was not observed for CAA 40-0, which can be related to the better mass transfer throughout its structure. In the detailed pictures of this work, a certain coalescence between the core particles can be appreciated for CAA 20-20 and CAA 0-40, creating larger particles, but also larger interparticular pores. However, the pieces preserved their integrity and showed a higher crushing resistance, as previously detailed.

3.2. Energy storage capacity of the materials after cycling

The obtained pellets were tested in 15 cycles of decarbonation/carbonation at $850/600 \text{ }^\circ\text{C}$ respectively in TG to assess their respective performance as prospective materials for thermochemical energy storage in CSP plants. Thus, the chosen experimental conditions for TG cycles were based on those proposed for CSP tower plants integrating CaL (Edwards and Materić, 2012). In these TG experiments, the formation of mayenite reduces the amount of CaO that can react with CO_2 . However, the actual amount of remaining CaO or mayenite cannot be easily determined by conventional techniques and, hence, the yield of carbonation (X_e) is herein referred to the initial CaO content of the samples and it is shown in Fig. 6. CAA 40-0 pellet, where all the alumina

Table 2

Energy storage capacity (kJ/kg) and crushing hardness (N) of CaO-based pellets reported in the literature.

Pellets ^a	Reaction conditions ^b	Number of cycles/reactor ^c	Energy storage capacity (kJ/kg) in last cycle	Crushing strength (N)	Ref.
CaO doped with 5% bagasse	Carbonation: $800 \text{ }^\circ\text{C}$, CO_2 , 10 min, 13 bar Calcination: $950 \text{ }^\circ\text{C}$, CO_2 , 10 min, 1 bar	10, DFR	860	4.0	Li et al. (2020)
CaO doped with 10% bagasse + 5% Al_2O_3	Carbonation: $850 \text{ }^\circ\text{C}$, CO_2 , 10 min Calcination ^d : $850 \text{ }^\circ\text{C}$, N_2	30, BFR	1621	5.0	Zhangke et al. (2021)
CaO doped with 20% cellulose	Carbonation: $850 \text{ }^\circ\text{C}$, CO_2 , 6 min Calcination: $750 \text{ }^\circ\text{C}$, CO_2 , 10 min	20, TGA	1720	5.3	Bai et al. (2021)
CaO doped with 20% cellulose and 25% TiO_2	Carbonation: $850 \text{ }^\circ\text{C}$, CO_2 , 10 min Calcination: $750 \text{ }^\circ\text{C}$, N_2 , 25 min	20, TGA	1827	7.3	
CaO doped with 35% Y_2O_3	Carbonation: $850 \text{ }^\circ\text{C}$, CO_2 , 10 min Calcination: $750 \text{ }^\circ\text{C}$, N_2 , 25 min	10, DFR	1872	n/a ^e	Li et al. (2021)
CaCO_3 doped with 20% Al (molar) and 60% cellulose	Carbonation: $800 \text{ }^\circ\text{C}$, 50% CO_2 , 15min Calcination: $800 \text{ }^\circ\text{C}$, N_2 , 15 min	20, TGA	1016	3.0	Xinrui et al. (2023)
CaO doped with 6.7% Zr, 6% Mn, 12% Fe (molar)	Carbonation: $850 \text{ }^\circ\text{C}$, 90% CO_2 , 6 min Calcination: $950 \text{ }^\circ\text{C}$, 90% CO_2 , 5 min	19, TGA	1000	3.4	Sun et al. (2022)
CaCO_3 doped with 15% Al, 5% Mn, 10% Fe, 10% Li_2CO_3 (molar)	Carbonation: $725 \text{ }^\circ\text{C}$, 50% CO_2 , 20min Calcination: $725 \text{ }^\circ\text{C}$, 100% N_2 , 15min	60, TGA	1671	1.9	Liu et al. (2022)
CaO doped with 5% Zr	Carbonation: $800 \text{ }^\circ\text{C}$, CO_2 , 10 min Calcination: $950 \text{ }^\circ\text{C}$, CO_2 , 10 min	20, TGA	1280	<2	Zhou et al. (2021)
CaO doped with 30% Zr	Carbonation: $800 \text{ }^\circ\text{C}$, CO_2 , 10 min Calcination: $950 \text{ }^\circ\text{C}$, CO_2 , 10 min	20, TGA	1150	8.3	
CAA 40-0	Carbonation: $600 \text{ }^\circ\text{C}$, N_2	15, TGA	1011	<5	This work
CAA 20-20	Calcination: $50 \text{ }^\circ\text{C}$, CO_2	15, TGA	1030	24	
CAA 20-20 M	Calcination: $850 \text{ }^\circ\text{C}$, CO_2	50, TGA	873	37	

^a All percentages are expressed in weight unless stated otherwise.

^b Pressure is 1 bar when not stated. Reaction time at constant temperature was only allowed when stated.

^c DFR: Dual fixed bed reactor; BFR: bubbling fluidized bed reactor; TGA: thermobalance.

^d Calcination step was performed until no CO_2 was detected at the reactor outlet.

^e Only attrition resistance experiments were carried out.

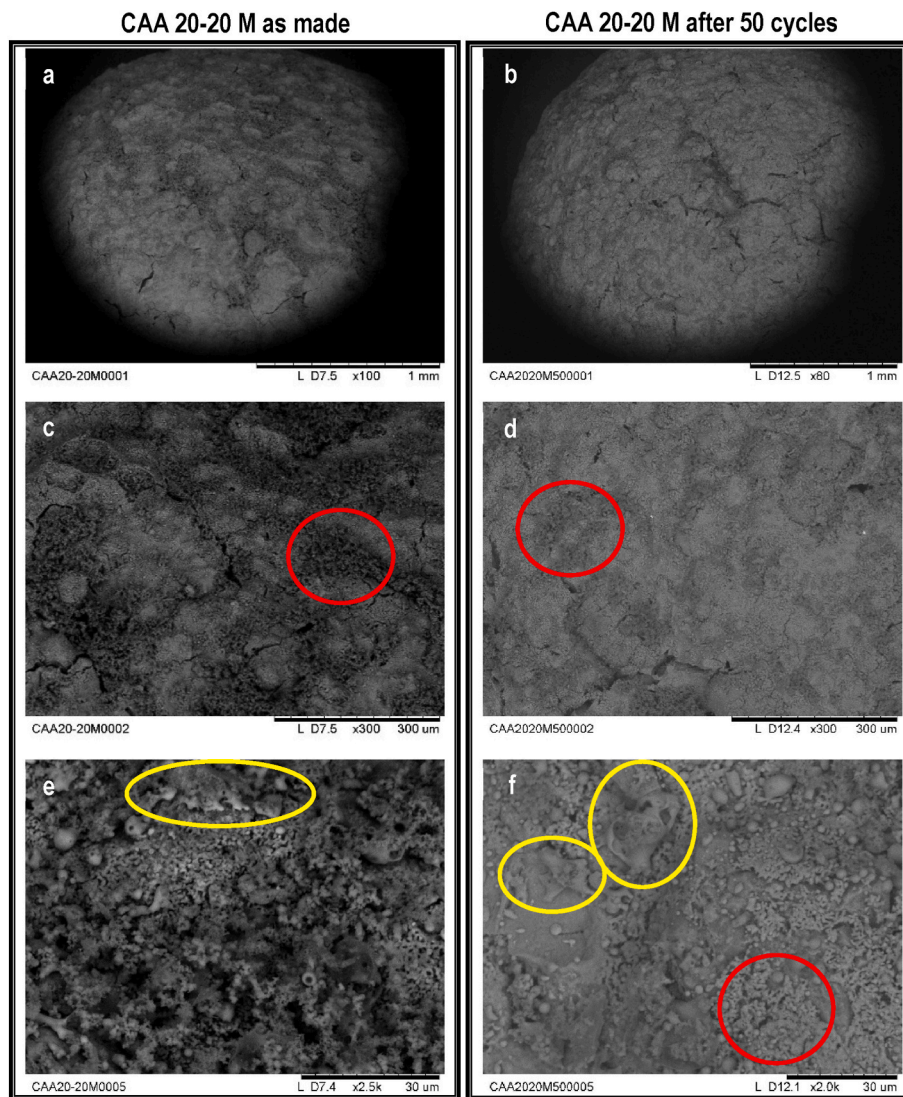


Fig. 7. SEM images of the coated CAA 20-20 M (60% Ca(OH)_2 / 20% $\gamma\text{-Al}_2\text{O}_3$ / 20% $m\text{-Al}_2\text{O}_3$) pellet before and after 50 carbonation/decarbonation cycles.

is commercial, exhibited a high carbonation yield of 0.7 in the first cycle, indicating that 70% of the calcium oxide present in the sample is successfully carbonated. This value underwent a decrease as the number of carbonation/calcination cycles was increased, stabilizing at 0.53 after 15 cycles. The replacement of commercial alumina by mesoporous alumina resulted in lower carbonation yield than CAA 40-0, though the values observed after 15 cycles are analogous when the amount of mesoporous alumina is moderate (CAA 30-10 and CAA 20-20). The effect of $m\text{-Al}_2\text{O}_3$ content was more pronounced as its amount was increased. Samples displayed progressively lower carbonation yield values, being of 0.49 and 0.38 for CAA 10-30 and CAA 0-40 pellets respectively after 15 cycles. These results are in agreement with the smaller amount of calcium oxide available for reaction with CO_2 after being transformed in mayenite by reacting with mesoporous alumina. Additionally, in the cases of CAA 30-10 and CAA 20-20 samples, the formation of mayenite slows down the quick decay in carbonation yield typically observed after cycling. This is indicative of a lower sintering of the calcium carbonate particles, hindering the appearance of the external passivating layer of calcium carbonate that delays heavily the diffusion of CO_2 inside the particle (Benitez-Guerrero et al., 2017, 2018a). This fact turns these materials into a rather stable ones for energy storage applications. On the other hand, the loss of porosity may be hindering the access of CO_2 to the available reactive calcium oxide

centers. Nevertheless, the loss of the porous structure does not imply that all remaining CaO in the pellet is unavailable for calcium looping. CO_2 can still diffuse through large gaps or cracks, although this diffusion is expected to be limited to the closest proximities of the voids. Energy storage density follows a similar pattern, with values obtained after 15 cycles ranging from 1030 kJ/kg to 731 kJ/kg corresponding to samples CAA 40-0 and CAA 0-40 respectively.

The presence of mesoporous alumina in the pellet core maintains the trend in the conversion of CaO to CaCO_3 after the 15 carbonation/calcination cycles while increasing its crushing strength from values below 5 N (sample CAA 40-0) to 24 N (sample 20-20), as can be seen in Fig. 2 above.

Table 2 lists thermal storage density and crushing strength of CaO -based pellets reported in the literature. Some of them use organic materials such as bagasse or cellulose to generate holes within the pellet structure, enhancing gas diffusion but fragilizing the pellet (Bai et al., 2021). Without going into specific details of each work, several doping agents are used to increase pellet crushing resistance, i.e., Al, Ti, Y, Zr, Mn, and Fe, generating mixed oxides with high Tamman temperature. These compounds space CaO grains and strengthen pellet structures, inhibiting the migration and subsequent sintering of CaO grains. However, excessive amounts of doping agent reduce the quantity of active calcium oxide, thus lowering energy storage capacity. The optimum

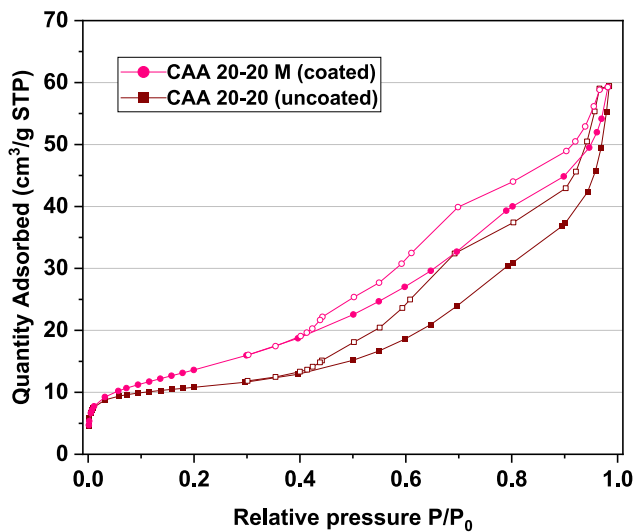


Fig. 8. N_2 adsorption-desorption isotherms at -196.15 °C of the calcined uncoated CAA 20-20 and coated CAA 20-20 M pellets (60 wt % $Ca(OH)_2$ /20 wt % $\gamma-Al_2O_3$ /20 wt % $m-Al_2O_3$).

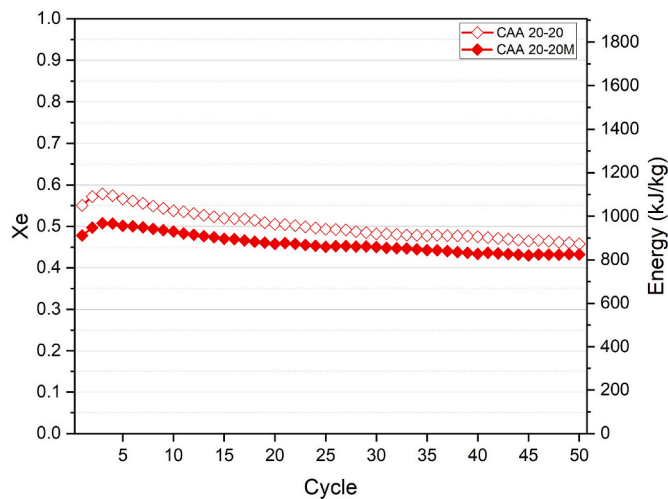


Fig. 9. Carbonation yield (X_c) (left) and energy storage density (kJ/kg) (right) of the uncoated CAA 20-20 and coated CAA 20-20M pellets (60 wt % $Ca(OH)_2$ /20 wt % $\gamma-Al_2O_3$ /20 wt % $m-Al_2O_3$) along 50 carbonation/decarbonation cycles.

values listed in Table 1 show that the best result of the present work (1030 kJ/kg, sample CAA 20-20) is surpassed by several other pellet formulations. However, the crushing strength of these pellets ranges from 2 N to 7.3 N, values three-fold smaller than the 24 N corresponding to CAA 20-20. Hence, this sample combines a remarkable crushing strength with a considerable energy storage density.

3.3. Long-term cycling for chosen materials

From the previous results, the CAA 20-20 material was selected as the most promising calcium oxide-binder combination for Calcium Looping applications in CSP plants since it showed the best compromise between textural properties, mechanical stability, and performance in the decarbonation/carbonation cycles. All these properties gave rise to a high and sustained energy storage capacity above 1000 kJ/kg in 15-cycle Calcium Looping experiments in TG. In addition, for an actual application, the bare CAA 20-20 cores might be covered by a shell that

can prevent further the attrition and disaggregation of the pellets during operation. In a previous work of dehydration/hydration cycles, a thin porous-silica coating produced by a dip-coating method (Briones et al., 2022) provided extra hardness by the formation of calcium silicate or calcium aluminosilicate and prevented loss of material, while aiding diffusion to and from the pellets by the formation of a porous external layer. Thus, the CAA 20-20 pellets were coated with porous silica-alumina and the formed material, named as CAA 20-20 M, was characterized again, and tested in longer 50-cycle experiments.

Fig. 7 shows a collection of SEM images on CAA 20-20 M before and after the 50 cycles of decarbonation/carbonation experiments. The porous coating is made of small silica-alumina grains that decorate the external surface of the pellet. Some of the more apparent fragments of silica grains have been indicated with red circles in figure. A more continuous layer (circled in yellow) can be devised in the detailed pictures (images e and f), especially in the after-cycles piece. This is ascribed to a mixed calcium-silicon phase, since the formation of calcium silicate in similar materials have been reported before (Sun et al., 2014). The formation of a such a mixed phase, firstly during the calcination of the samples, and then during the cycles, would explain why the silica grains are less visible in the images taken after the experiment. Evidence of the aforementioned phases being silica based was provided by EDX analyses as shown in Fig. S1 of the Supporting Information. It has to be mentioned that no residual powder was collected in the crucibles after the experiments and thus the partial detaching of the coating was ruled out. Besides, the extension of the coating seems to be unchanged after the experiment. As for the integrity of the pieces, it is clear that long-term experiments do not cause additional surface cracking or breakage.

The presence of a crystalline calcium silicate in the pellets cannot be corroborated by XRD, due to the very small amount that can be derived from the thin layer of coating. However, Ca-Si-Al mixed phases have been shown before to be formed by calcination at 500 °C of calcium hydroxide mixed with the gel conducting to porous silica (Briones et al., 2022). Since silicates are hard materials, an increase in the resistance to crushing of the coated materials is expected compared to the bare cores. In this case, the CAA 20-20 pellets displayed an average measurement of 24 ± 8 N (Fig. 2), and the coated CAA 20-20 M provided a value of 37 ± 6 N.

Comparing the unreacted CAA 20-20 M with its uncoated counterpart (Fig. 7 e and Fig. 7 b and 7 e) it seems that the outer surface of CAA 20-20 M is rougher, with larger particles but also larger voids. In a similar fashion as what was described for the formation of mayenite, the formation of silicates causes the sintering of some particles without collapsing the porous structure and, therefore, some larger pores are created. To check if the coating affected the textural properties, nitrogen physisorption was also performed on the CAA 20-20 M material. The adsorption-desorption isotherms of the coated and uncoated samples are represented in Fig. 8. The isotherm of CAA 20-20 M is slightly above the one corresponding to the uncoated sample, with a BET surface area of $50 \text{ m}^2/\text{g}$ and total volume of pores of $0.09 \text{ cm}^3/\text{g}$. Thus, the accessibility of the coated sample does not seem to be compromised.

These pellets were subjected to 50 cycles of carbonation/calcination, with the carbonation yields being shown in Fig. 9. First, it can be observed that the decrease in the carbonation yield continues after 15 cycles through a slight but continuous process, reaching a value of 0.46 for CAA 20-20 after the 50 cycles, which corresponds to 84 % of the yield observed in the first cycle.

Coated sample CAA 20-20 M achieved yield values of 0.48 and 0.43 after the first and last cycle of the series respectively, maintaining 90 % of the initial yield after 50 cycles. Comparing both samples, pellet coating shows a slight negative influence on the carbonation reaction, hindering gas diffusion, but significantly increases pellet strength from 24 N to 37 N. It is particularly noteworthy the very small decay in carbonation performance after 50 cycles which is indicative again that the presence of mayenite in the pellets is able to reduce calcium oxide/

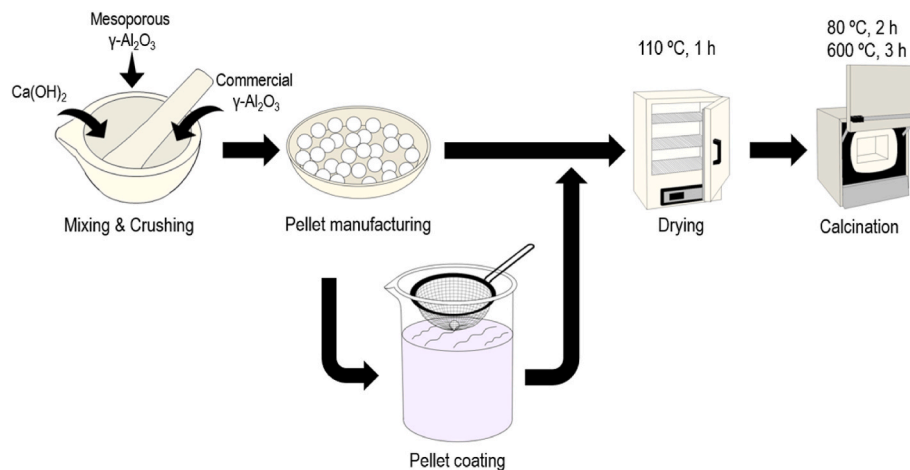


Fig. 10. Preparation procedure of coated and uncoated CAA pellets ($\text{Ca}(\text{OH})_2/\gamma\text{-Al}_2\text{O}_3/\text{m-Al}_2\text{O}_3$).

carbonate sintering in a very effective way. In this regard, mayenite occurrence plays indeed a two-fold role: a) to provide enhanced mechanical resistance to the pellet and b) to hold a rather stable carbonation performance along cycling. Additionally, the porous silica-alumina coating succeeds in beefing up the mechanical resistance of the pellet. These are both very promising features for the application of CAA 20-20 M as energy storage material in Calcium Looping for CSP plants. However, one limitation of this approach is the relatively large size of the CAA pellets (around 2.5–3 mm) which is likely excessive considering the usual sizes employed in the fluidized beds implementing CaL process (around 0.5–1 mm) (Zheng et al., 2023). In this respect, they are more in keeping with the sizes traditionally used in fixed/moving beds. Therefore, the future work will be aimed to attain pellets with smaller sizes more in agreement with the technical requirements of fluidized beds for CaL process.

By comparison of these findings with the most recent results published in literature, the preparation of MgO-stabilized CaO composites was reported with a carbonation yield of 0.46 g $\text{CO}_2/\text{g-composite}$ after 20 cycles and a striking energy storage density of 2219 kJ/kg (Huang et al., 2022). However, the crushing strength of these materials was just 1.43 N which renders them difficult for their practical implementation in CaL inside CSP plants. In addition, CaO-based pellets were prepared harnessing a binder solution of PVA (polyvinyl alcohol). These pellets displayed a high energy storage after 10 cycles (~2400 kJ/kg) and in the friability tests, they exhibited a 10 wt % loss after 2400 rotations (Xu et al., 2024). However, neither higher number of carbonation cycles nor crushing strengths of the pellets were provided, and along the studied ten cycles, these pellets showed a steady decrease in energy storage density which compromises their long-term performance. On the other hand, $\text{AlMgFeMnO}_x\text{CaCO}_3$ pellets were prepared that showed a remarkable long-term stability in energy storage density, holding more than 85% of the starting value after 100 cycles of carbonation/decarbonation, which corresponds to energy storage densities of ~1000 kJ/kg (Zheng et al., 2023). However, the average crushing strength of the pellets after cycling varied within the range 1.54–4.36 N, that is still low for obtaining prolonged performance. Interestingly, CaO based pellets prepared with cement and microcrystalline cellulose as binders were reported that showed energy storage densities of 1148 kJ/kg after 50 cycles of decarbonation/carbonation and a remarkable crushing strength of 14.63 N (Rong et al., 2024). These authors disclosed as well a steam injection treatment during calcination that led towards higher crushing strengths of the pellets (27.05 N) but at the expense of losing energy storage density after 50 cycles (826 kJ/kg). These latter results are in keeping with those present in this work and they bear out it is feasible to attain CaO – based pellets with high energy storage densities (>800 kJ/kg) after long-term carbonation/decarbonation cycling

while holding high crushing strengths too. This is a guarantee of enhanced resistance to attrition and it constitutes an important landmark for the practical implementation of CaL in CSP plants. On the other hand, CAA pellets may help the development of the third generation CSP plants that are characterized by using higher maximum cycle temperatures and need modern materials to address heat transmission and thermal storage under these more stringent conditions (Alami et al., 2023). This feature allows them to achieve annual solar-electric efficiencies of 25–30%, instead of the lower ~9–16% of the first generation CSP plants and ~10–20% of the second generation ones (He et al., 2020). This is particularly interesting considering that, according to International Energy Agency, CSP might furnish 3.0–3.6 % of the global energy supply for 2030 and this amount is expected to hike to 8–11.8% for 2050 (Alami et al., 2023).

4. Conclusions

This study demonstrates the viability of mesoporous alumina ($\text{m-Al}_2\text{O}_3$) as an effective binder component to enhance the CaO-based pellet crushing strength while holding a remarkable energy storage density. The high BET surface area of mesoporous $\gamma\text{-Al}_2\text{O}_3$ increased the interaction with the calcium oxide, leading towards the formation of mayenite which caused to augment the crushing strength of the pellet. Despite slightly decreasing CaO carbonation yields after cycling, the stability of $\text{m-Al}_2\text{O}_3$ -containing samples highlights their durability. In this regard, the formation of mayenite facilitated by $\text{m-Al}_2\text{O}_3$ presence not only increases the mechanical resistance of the pellets but it slows down the carbonation yield decay due to the hindered sintering of calcium oxide/carbonate. In this respect, the optimum CAA 20-20 (60 wt % $\text{Ca}(\text{OH})_2/20$ wt % $\gamma\text{-Al}_2\text{O}_3/20$ wt % $\text{m-Al}_2\text{O}_3$) pellet achieved a remarkable carbonation yield of 0.46 after 50 cycles, which accounts for the 84% of its starting value and corresponds to an energy storage density of ~873 kJ/kg. In addition, the coating of the CAA 20-20 pellet with a porous silica-alumina layer (CAA 20-20 M pellet) further improved the crushing strength without compromising textural properties and with only a slight decrease in carbonation yields and energy storage density. Hence, the CAA 20-20 M composition proved an excellent trade-off between reactivity and mechanical stability, showing a strength of 37 N and a calcium oxide carbonation yield of 0.43 after 50 cycles, corresponding to an energy storage density of ~824 kJ/kg. These findings support the application of these CaO-based pellets in Calcium Looping technology inside the third generation CSP plants which require materials with large and durable storage capacity at the higher maximum temperatures (>600 °C) of the cycles, in order to attain enhanced solar-electric efficiencies up to 25–30%. In this respect, these CaO-based pellets may be a promising contribution to fulfill the goal of

the practical implementation of the third generation CSP plants setting up the CaL process.

CRediT authorship contribution statement

D. Castro-Yáñez: Writing - original draft, Investigation, Data curation, Conceptualization, Methodology, Formal analysis. **M. Erans:** Investigation, Conceptualization. **A. Peral:** Writing – review & editing, Validation. **R. Sanz:** Writing – review & editing, Validation. **J. González-Aguilar:** Writing – review & editing, Funding acquisition. **M. Romero:** Writing – review & editing, Funding acquisition. **L. Briones:** Writing – original draft, Visualization, Methodology, Investigation, Formal analysis, Conceptualization. **E.S. Sanz-Pérez:** Writing – review & editing, Writing – original draft, Software, Resources, Project administration. **J.M. Escola:** Writing – review & editing, Writing – original draft, Validation, Supervision, Formal analysis.

Declaration of competing interest

The authors declare that they have no known competing financial interests or personal relationships that could have appeared to influence the work reported in this paper.

Data availability

Data will be made available on request.

Acknowledgements

M.E. is grateful for Grant *RYC2021-031428-I* funded by MCIN/AEI/10.13039/501100011033 and by European Union NextGenerationEU/PRTR. The authors wish to thank Comunidad de Madrid and European Structural Funds for their financial support to ACES2030-CM project (S2018/EMT-4319).

Appendix A. Supplementary data

Supplementary data to this article can be found online at <https://doi.org/10.1016/j.jclepro.2024.141702>.

References

- Abanades, J.C., Anthony, E.J., Wang, J., Oakey, J.E., 2005. Fluidized bed combustion systems integrating CO₂ capture with CaO. *Environ. Sci. Technol.* 39, 2861–2866. <https://doi.org/10.1021/ES0496221/ASSET/IMAGES/LARGE/ES0496221F00006.JPG>.
- Abedin, A.H., 2011. A critical review of thermochemical energy storage systems. *Open Renew. Energy J.* 4, 42–46. <https://doi.org/10.2174/1876387101004010042>.
- Aguado, J., Escola, J.M., Castro, M.C., 2010. Influence of the thermal treatment upon the textural properties of sol-gel mesoporous γ -alumina synthesized with cationic surfactants. *Microporous Mesoporous Mater.* 128, 48–55. <https://doi.org/10.1016/J.MICROMESO.2009.08.002>.
- Aguado, J., Escola, J.M., Castro, M.C., Paredes, B., 2005. Sol-gel synthesis of mesostructured γ -alumina templated by cationic surfactants. *Microporous Mesoporous Mater.* 83, 181–192. <https://doi.org/10.1016/J.MICROMESO.2005.03.021>.
- Alami, A.H., Olabi, A.G., Mdallal, A., Rezk, A., Radwan, A., Rahman, S.M.A., Shah, S.K., Abdelkareem, M.A., 2023. Concentrating solar power (CSP) technologies: status and analysis. *Int. J. Thermofluid.* 18, 100340. <https://doi.org/10.1016/J.IJTF.2023.100340>.
- Alovisio, A., Chacartegui, R., Ortiz, C., Valverde, J.M., Verda, V., 2017. Optimizing the CSP-calcium looping integration for thermochemical energy storage. *Energy Convers. Manag.* 136, 85–98. <https://doi.org/10.1016/J.ENCONMAN.2016.12.093>.
- Álvarez Criado, Y., Alonso, M., Abanades, J.C., 2015. Composite material for thermochemical energy storage using CaO/Ca(OH)₂. *Ind. Eng. Chem. Res.* 54, 9314–9327. <https://doi.org/10.1021/acs.iecr.5b02688>.
- Bai, S., Sun, J., Zhou, Z., Bu, C., Chen, X., Yang, Y., Wang, R., Guo, Y., Zhao, C., Liu, W., 2021. Structurally improved, TiO₂-incorporated, CaO-based pellets for thermochemical energy storage in concentrated solar power plants. *Sol. Energy Mater. Sol. Cell.* 226. <https://doi.org/10.1016/j.solmat.2021.111076>.
- Barrett, E.P., Joyner, L.G., Halenda, P.P., 1951. The determination of pore volume and area distributions in porous substances. I. Computations from nitrogen isotherms. *J. Am. Chem. Soc.* 73, 373–380. <https://doi.org/10.1021/JA01145A126/ASSET/JA01145A126.FP.PNG.V03>.
- Bell, S., Steinberg, T., Will, G., 2019. Corrosion mechanisms in molten salt thermal energy storage for concentrating solar power. *Renew. Sustain. Energy Rev.* 114, 109328. <https://doi.org/10.1016/J.RSER.2019.109328>.
- Benitez-Guerrero, M., Valverde, J.M., Perejon, A., Sanchez-Jimenez, P.E., Perez-Maqueda, L.A., 2018a. Low-cost Ca-based composites synthesized by biotemplate method for thermochemical energy storage of concentrated solar power. *Appl. Energy* 210, 108–116. <https://doi.org/10.1016/j.apenergy.2017.10.109>.
- Benitez-Guerrero, M., Valverde, J.M., Sanchez-Jimenez, P.E., Perejon, A., Perez-Maqueda, L.A., 2018b. Calcium-Looping performance of mechanically modified Al₂O₃-CaO composites for energy storage and CO₂ capture. *Chem. Eng. J.* 334, 2343–2355. <https://doi.org/10.1016/j.cej.2017.11.183>.
- Benitez-Guerrero, M., Valverde, J.M., Sanchez-Jimenez, P.E., Perejon, A., Perez-Maqueda, L.A., 2017. Multicycle activity of natural CaCO₃ minerals for thermochemical energy storage in Concentrated Solar Power plants. *Sol. Energy* 153, 188–199. <https://doi.org/10.1016/j.solener.2017.05.068>.
- Bian, Z., Li, Y., Ren, Y., Fang, Y., Zhao, J., 2022. Thermochemical heat storage performance of CaO particles under fluidization in coupled CaO/Ca(OH)₂ cycles and CaO/CaCO₃ cycles. *J. Energy Storage* 56, 106045. <https://doi.org/10.1016/J.EST.2022.106045>.
- Blamey, J., Anthony, E.J., Wang, J., Fennell, P.S., 2010. The calcium looping cycle for large-scale CO₂ capture. *Prog. Energy Combust. Sci.* 36, 260–279. <https://doi.org/10.1016/J.PECS.2009.10.001>.
- Boyu, L., Yingjie, L., Yehui, D., Yuzhuo, W., Jianli, Z., Tao, W., 2021. SiC/Mn co-doped CaO pellets with enhanced optical and thermal properties for calcium looping thermochemical heat storage. *Chem. Eng. J.* 423, 130305.
- Briones, L., Valverde-Pizarro, C.M., Barras-García, I., Tajuelo, C., Sanz-Pérez, E.S., Sanz, R., Escola, J.M., González-Aguilar, J., Romero, M., 2022. Development of stable porous silica-coated Ca(OH)₂/ γ -Al₂O₃ pellets for dehydration/hydration cycles with application in thermochemical heat storage. *J. Energy Storage* 51, 104548. <https://doi.org/10.1016/j.est.2022.104548>.
- Broda, M., Müller, C.R., 2014. Sol-gel-derived, CaO-based, ZrO₂-stabilized CO₂ sorbents. *Fuel* 127, 94–100. <https://doi.org/10.1016/J.FUEL.2013.08.004>.
- Brunauer, S., Emmett, P.H., Teller, E., 1938. Adsorption of gases in multimolecular layers. *J. Am. Chem. Soc.* 60, 309–319. <https://doi.org/10.1021/JA01269A023/ASSET/JA01269A023.FP.PNG.V03>.
- Carrillo, A.J., González-Aguilar, J., Romero, M., Coronado, J.M., 2019. Solar energy on demand: a review on high temperature thermochemical heat storage systems and materials. *Chem. Rev.* 119, 4777–4816. <https://doi.org/10.1021/ACS.CHEMREV.8B00315>.
- Chacartegui, R., Alovisio, A., Ortiz, C., Valverde, J.M., Verda, V., Becerra, J.A., 2016. Thermochemical energy storage of concentrated solar power by integration of the calcium looping process and a CO₂ power cycle. *Appl. Energy* 173, 589–605. <https://doi.org/10.1016/J.APENERGY.2016.04.053>.
- Chen, H., Zhang, P., Duan, Y., Zhao, C., 2016a. Reactivity enhancement of calcium based sorbents by doped with metal oxides through the sol-gel process. *Appl. Energy* 162, 390–400. <https://doi.org/10.1016/J.APENERGY.2015.10.035>.
- Chen, H., Zhang, P., Duan, Y., Zhao, C., 2016b. CO₂ capture of calcium based sorbents developed by sol-gel technique in the presence of steam. *Chem. Eng. J.* 295, 218–226. <https://doi.org/10.1016/J.CEJ.2016.03.008>.
- Chen, H., Zhao, C., Yang, Y., Zhang, P., 2012. CO₂ capture and attrition performance of CaO pellets with aluminate cement under pressurized carbonation. *Appl. Energy* 91, 334–340. <https://doi.org/10.1016/j.apenergy.2011.09.032>.
- Chen, R., Romero, M., González-Aguilar, J., Rovense, F., Rao, Z., Liao, S., 2022. Optical and thermal integration analysis of supercritical CO₂ Brayton cycles with a particle-based solar thermal plant based on annual performance. *Renew. Energy* 189, 164–179. <https://doi.org/10.1016/J.RENENE.2022.02.059>.
- Chen, X., Jin, X., Liu, Z., Ling, X., Wang, Y., 2018. Experimental investigation on the CaO/CaCO₃ thermochemical energy storage with SiO₂ doping. *Energy* 155, 128–138. <https://doi.org/10.1016/J.ENERGY.2018.05.016>.
- Choi, S., Drese, J.H., Jones, C.W., 2009. Adsorbent materials for carbon dioxide capture from large anthropogenic point sources. *ChemSusChem* 2, 796–854. <https://doi.org/10.1002/CSSC.200900036>.
- Da, Y., Zhou, J., 2022. Multi-doping strategy modified calcium-based materials for improving the performance of direct solar-driven calcium looping thermochemical energy storage. *Sol. Energy Mater. Sol. Cell.* 238, 111613. <https://doi.org/10.1016/J.SOLMAT.2022.111613>.
- Edwards, S.E.B., Materić, V., 2012. Calcium looping in solar power generation plants. *Sol. Energy* 86, 2494–2503. <https://doi.org/10.1016/J.SOLENER.2012.05.019>.
- Erans, M., Manovic, V., Anthony, E.J., 2016. Calcium looping sorbents for CO₂ capture. *Appl. Energy* 180, 722–742. <https://doi.org/10.1016/J.APENERGY.2016.07.074>.
- Ervin, G., 1977. Solar heat storage using chemical reactions. *J. Solid State Chem.* 22, 51–61. [https://doi.org/10.1016/0022-4596\(77\)90188-8](https://doi.org/10.1016/0022-4596(77)90188-8).
- García-Ferrero, J., Merchán, R.P., Santos, M.J., Medina, A., Calvo Hernández, A., 2022. Brayton technology for Concentrated Solar Power plants: comparative analysis of central tower plants and parabolic dish farms. *Energy Convers. Manag.* 271. <https://doi.org/10.1016/J.ENCONMAN.2022.116312>.
- Gil, A., Medrano, M., Martorell, I., Lázaro, A., Dolado, P., Zalba, B., Cabeza, L.F., 2010. State of the art on high temperature thermal energy storage for power generation. Part 1-Concepts, materials and modelization. *Renew. Sustain. Energy Rev.* 14, 31–55. <https://doi.org/10.1016/J.RSER.2009.07.035>.
- Gollsch, M., Linder, M., 2023. Influence of structural changes on gas transport properties of a cycled CaO/Ca(OH)₂ powder bulk for thermochemical energy storage. *J. Energy Storage* 73. <https://doi.org/10.1016/J.EST.2023.108790>.

- Grasa, G.S., Abanades, J.C., 2006. CO₂ capture capacity of CaO in long series of carbonation/calcination cycles. *Ind. Eng. Chem. Res.* 45, 8846–8851. <https://doi.org/10.1021/IE0606946/ASSET/IMAGES/MEDIUM/IE0606946E00005.GIF>.
- Hasnain, S.M., 1998. Review on sustainable thermal energy storage technologies, part I: heat storage materials and techniques. *Energy Convers. Manag.* 39, 1127–1138. [https://doi.org/10.1016/S0196-8904\(98\)00025-9](https://doi.org/10.1016/S0196-8904(98)00025-9).
- He, Y.L., Qiu, Y., Wang, K., Yuan, F., Wang, W.Q., Li, M.J., Guo, J.Q., 2020. Perspective of concentrating solar power. *Energy* 198, 117373. <https://doi.org/10.1016/J.ENERGY.2020.117373>.
- Huang, C., Xu, M., Huai, X., Liu, Z., 2022. Hierarchically porous calcium-based composites synthesized by eggshell membrane templating for thermochemical energy storage of concentrated solar power. *J. Energy Storage* 52, 104769. <https://doi.org/10.1016/J.EST.2022.104769>.
- Islam, M.T., Huda, N., Abdullah, A.B., Saidur, R., 2018. A comprehensive review of state-of-the-art concentrating solar power (CSP) technologies: current status and research trends. *Renew. Sustain. Energy Rev.* 91, 987–1018. <https://doi.org/10.1016/J.RSER.2018.04.097>.
- Kierzkowska, A.M., Pacciani, R., Müller, C.R., 2013. CaO-based CO₂ sorbents: from fundamentals to the development of new, highly effective materials. *ChemSusChem* 6, 1130–1148. <https://doi.org/10.1002/CSSC.201300178>.
- Lambrecht, M., de Miguel, M.T., Lasanta, M.I., Pérez, F.J., 2022. Past research and future strategies for molten chlorides application in concentrated solar power technology. *Sol. Energy Mater. Sol. Cell.* 237, 111557. <https://doi.org/10.1016/J.SOLMAT.2021.111557>.
- Li, B., Li, Y., Sun, H., Wang, Y., Wang, Z., 2020. Thermochemical heat storage performance of CaO pellets fabricated by extrusion-spherulization under harsh calcination conditions. *Energy & Fuels* 34, 6462–6473.
- Li, H., Chen, Y., Leng, L., Hu, Y., 2021. Thermochemical energy storage of concentrated solar power by novel Y₂O₃-doped CaO pellets. *Energy Fuel* 35, 12610–12618. <https://doi.org/10.1021/ACS.ENERGYFUELS.1C01270/ASSET/IMAGES/MEDIUM/EF1C01270.0015.GIF>.
- Lin, W., Cai, Q., Pang, W., Yue, Y., Zou, B., 1999. New mineralization agents for the synthesis of MCM-41. *Microporous Mesoporous Mater.* 33, 187–196. [https://doi.org/10.1016/S1387-1811\(99\)00137-7](https://doi.org/10.1016/S1387-1811(99)00137-7).
- Liu, D., Xin-Feng, L., Bo, L., Si-quan, Z., Yan, X., 2018. Progress in thermochemical energy storage for concentrated solar power: a review. *Int. J. Energy Res.* 42, 4546–4561. <https://doi.org/10.1002/ER.4183>.
- Liu, F.J., Chou, K.S., Huang, Y.K., 2006. A novel method to make regenerable core-shell calcium-based sorbents. *J. Environ. Manag.* 79, 51–56. <https://doi.org/10.1016/j.jenvman.2005.05.013>.
- Liu, X., Yuan, C., Zheng, H., Song, C., Tian, C., Gao, K., Sun, N., Jiang, Z., Xuan, Y., Ding, Y., 2022. Synergy of Li₂CO₃ promoters and Al-Mn-Fe stabilizers in CaCO₃ pellets enables efficient direct solar-driven thermochemical energy storage. *Mater. Today Energy* 30, 101174.
- Manovic, V., Anthony, E.J., 2011. Reactivation and remaking of calcium aluminate pellets for CO₂ capture. *Fuel* 90, 233–239. <https://doi.org/10.1016/j.fuel.2010.07.054>.
- Morona, L., Erans, M., Hanak, D.P., 2019. Effect of seawater, aluminate cement, and alumina-rich spinel on pelletized CaO-based sorbents for calcium looping. *Ind. Eng. Chem. Res.* 58, 11910–11919. <https://doi.org/10.1021/ACS.IECR.9B00944/ASSET/IMAGES/LARGE/IE-2019-009449.0017.JPEG>.
- Müller, B., Arlt, W., Wasserscheid, P., 2011. A new concept for the global distribution of solar energy: energy carrying compounds. *Energy Environ. Sci.* 4, 4322–4331. <https://doi.org/10.1039/C1EE01595H>.
- Opolot, M., Zhao, C., Liu, M., Mancin, S., Bruno, F., Hooman, K., 2022. A review of high temperature (≥ 500 °C) latent heat thermal energy storage. *Renew. Sustain. Energy Rev.* 160, 112293. <https://doi.org/10.1016/J.RSER.2022.112293>.
- Ortiz, C., Valverde, J.M., Chacartegui, R., Perez-Maqueda, L.A., Giménez, P., 2019. The Calcium-Looping (CaCO₃/CaO) process for thermochemical energy storage in Concentrating Solar Power plants. *Renew. Sustain. Energy Rev.* 113, 109252. <https://doi.org/10.1016/J.RSER.2019.109252>.
- Pardo, P., Deydier, A., Anxionnaz-Minvielle, Z., Rougé, S., Cabassud, M., Cognet, P., 2014. A review on high temperature thermochemical heat energy storage. *Renew. Sustain. Energy Rev.* 32, 591–610. <https://doi.org/10.1016/J.RSER.2013.12.014>.
- Perejón, A., Romeo, L.M., Lara, Y., Lisbona, P., Martínez, A., Valverde, J.M., 2016. The Calcium-Looping technology for CO₂ capture: on the important roles of energy integration and sorbent behavior. *Appl. Energy* 162, 787–807. <https://doi.org/10.1016/J.APENENERGY.2015.10.121>.
- Prieto, C., Cooper, P., Fernández, A.L., Cabeza, L.F., 2016. Review of technology: thermochemical energy storage for concentrated solar power plants. *Renew. Sustain. Energy Rev.* 60, 909–929. <https://doi.org/10.1016/J.RSER.2015.12.364>.
- Rea, J.E., Oshman, C.J., Olsen, M.L., Hardin, C.L., Glatzmaier, G.C., Siegel, N.P., Parilla, P.A., Ginley, D.S., Toberer, E.S., 2018. Performance modeling and techno-economic analysis of a modular concentrated solar power tower with latent heat storage. *Appl. Energy* 217, 143–152. <https://doi.org/10.1016/J.APENENERGY.2018.02.067>.
- Rong, N., Mu, Z., Shao, J., Liu, K., Han, L., Wang, S., Shi, X., Wang, G., 2024. Calcium-looping thermochemical energy storage and mechanical performance of bio-templated CaO-based pellets under steam-containing environments. *J. Energy Storage* 80, 110377. <https://doi.org/10.1016/J.EST.2023.110377>.
- Salvador, C., Lu, D., Anthony, E.J., Abanades, J.C., 2003. Enhancement of CaO for CO₂ capture in an FBC environment. *Chem. Eng. J.* 96, 187–195. <https://doi.org/10.1016/J.CEJ.2003.08.011>.
- Sedghkarder, M.H., Mahinpey, N., Soleimanisalim, A.H., Sun, Z., Chen, Z., Lim, J., Kaliaguine, S., 2016. Core-shell structured CaO-based pellets protected by mesoporous ceramics shells for high-temperature CO₂ capture. *Can. J. Chem. Eng.* 94, 2038–2044. <https://doi.org/10.1002/cjce.22626>.
- Shimizu, T., Hirama, T., Hosoda, H., Kitano, K., Inagaki, M., Tejima, K., 1999. A twin fluid-bed reactor for removal of CO₂ from combustion processes. *Chem. Eng. Res. Des.* 77, 62–68. <https://doi.org/10.1205/026387699525882>.
- Sun, H., Wang, J., Liu, X., Shen, B., Parlett, C.M.A., Adwek, G.O., John Anthony, E., Williams, P.T., Wu, C., 2019. Fundamental studies of carbon capture using CaO-based materials. *J. Mater. Chem. A Mater.* 7, 9977–9987. <https://doi.org/10.1039/C8TA10472G>.
- Sun, J., Bai, S., Li, K., Zhou, Y., Chen, Y., Liu, L., Zhou, Z., 2022. Evaluation of thermochemical energy storage performance of Fe-/Mn-doped, Zr-stabilized, CaO-based composites under different thermal energy storage modes. *ACS Appl. Energy Mater.* 5, 4903–4915. <https://doi.org/10.1021/ACSAEM.2C00303/ASSET/IMAGES/LARGE/AE2C00303.0014.JPEG>.
- Sun, J., Wang, W., Yang, Y., Cheng, S., Guo, Y., Zhao, C., Liu, W., Lu, P., 2020. Reactivation mode investigation of spent CaO-based sorbent subjected to CO₂ looping cycles or sulfation. *Fuel* 266, 117056. <https://doi.org/10.1016/J.FUEL.2020.117056>.
- Sun, R., Li, Y., Liu, H., Wu, S., Lu, C., 2012. CO₂ capture performance of calcium-based sorbent doped with manganese salts during calcium looping cycle. *Appl. Energy* 89, 368–373. <https://doi.org/10.1016/J.APENENERGY.2011.07.051>.
- Sun, Z., Sedghkarder, M.H., Saayman, J., Mahinpey, N., Ellis, N., Zhao, D., Kaliaguine, S., 2014. A Facile fabrication of mesoporous core-shell CaO-based pellets with enhanced reactive stability and resistance to attrition in cyclic CO₂ capture. *J. Mater. Chem. A* 2, 16577–16588. <https://doi.org/10.1039/C4TA03854A>.
- Valverde-Pizarro, C.M., Briones, L., Sanz, E., Escola, J.M., Sanz, R., González-Aguilar, J., Romero, M., 2020. Coating of Ca(OH)₂/γ-Al₂O₃ pellets with mesoporous Al₂O₃ and its application in thermochemical heat storage for CSP plants. *Renew. Energy* 162, 587–595. <https://doi.org/10.1016/j.renene.2020.08.095>.
- Vasu, A., Hagos, F.Y., Noor, M.M., Mamat, R., Azmi, W.H., Abdullah, A.A., Ibrahim, T.K., 2017. Corrosion effect of phase change materials in solar thermal energy storage application. *Renew. Sustain. Energy Rev.* 76, 19–33. <https://doi.org/10.1016/J.RSER.2017.03.018>.
- Wang, K., Gu, F., Clough, P.T., Zhao, P., Anthony, E.J., 2020. Porous MgO-stabilized CaO-based powders/pellets via a citric acid-based carbon template for thermochemical energy storage in concentrated solar power plants. *Chem. Eng. J.* 390, 124163. <https://doi.org/10.1016/J.CEJ.2020.124163>.
- Wang, S., Fan, S., Fan, L., Zhao, Y., Ma, X., 2015. Effect of cerium oxide doping on the performance of CaO-based sorbents during calcium looping cycles. *Environ. Sci. Technol.* 49, 5021–5027. <https://doi.org/10.1021/ES5052843/ASSET/IMAGES/LARGE/ES-2014-052843.0010.JPEG>.
- Xinrui, W., Xianglei, L., Hangbin, Z., Chao, S., Ke, G., Cheng, T., Nan, S., Zhixing, J., 2023. Hierarchically doping calcium carbonate pellets for directly solar-driven high-temperature thermochemical energy storage. *Sol. Energy* 251, 197–207.
- Xu, B., Fu, R., Liu, Y., Hu, Y., 2024. Fabrication of CaO pellets via polyvinyl alcohol (PVA) method for efficient CO₂ capture and solar energy storage. *Sep. Purif. Technol.* 335, 126135. <https://doi.org/10.1016/J.SEPPUR.2023.126135>.
- Xu, J., Wang, R.Z., Li, Y., 2014. A review of available technologies for seasonal thermal energy storage. *Sol. Energy* 103, 610–638. <https://doi.org/10.1016/J.SOLENER.2013.06.006>.
- Yan, T., Wang, R.Z., Li, T.X., Wang, L.W., Fred, I.T., 2015. A review of promising candidate reactions for chemical heat storage. *Renew. Sustain. Energy Rev.* 43, 13–31. <https://doi.org/10.1016/J.RSER.2014.11.015>.
- Zhangke, M., Yingjie, L., Zeyan, W., Tao, W., Wentao, L., 2021. Calcium looping heat storage performance and mechanical property of CaO-based pellets under fluidization. *Chin. J. Chem. Eng.* 36, 170–180.
- Zheng, H., Liu, X., Xuan, Y., Ding, Y., Flamant, G., 2023. Efficient direct solar-driven thermochemical energy storage of (AlMgFeMn)OxCaCO₃ pellets in a fluidized bed reactor. *Energy Convers. Manag.* 285, 116990. <https://doi.org/10.1016/J.ENCONMAN.2023.116990>.
- Zhou, Y., Zhou, Z., Liu, L., She, X., Xu, R., Sun, J., Xu, M., 2021. Enhanced thermochemical energy storage stability of CaO-based composite pellets incorporated with a Zr-based stabilizer. *Energy Fuel* 35, 18778–18788. <https://doi.org/10.1021/acs.energyfuels.1c02788>.
- Zhou, Z., Qi, Y., Xie, M., Cheng, Z., Yuan, W., 2012. Synthesis of CaO-based sorbents through incorporation of alumina/aluminate and their CO₂ capture performance. *Chem. Eng. Sci.* 74, 172–180. <https://doi.org/10.1016/J.CES.2012.02.042>.